

Radio-Continuum Study of the Nearby Sculptor Group Galaxies. Part 2: NGC 55 at $\lambda=20, 13, 6$ and 3 cm

Andrew N. O'Brien, Miroslav D. Filipović, Evan J. Crawford, Nicholas F. H. Tothill, Jordan D. Collier, Ain Y. De Horta, Graeme F. Wong, Danica Drašković, Jeff L. Payne • Thomas G. Pannuti, Jared P. Napier, Stephen A. Griffith, Wayne D. Staggs • Srdjan Kotuš

Abstract A series of new radio-continuum ($\lambda=20, 13, 6$ and 3 cm) mosaic images focused on the NGC 55 galactic system were produced using archived observational data from the Australia Telescope Compact Array. These new images are both very sensitive (down to $\text{rms}=33 \mu\text{Jy}$) and feature high angular resolution (down to $<4''$). Using these newly created images, 66 previously unidentified discrete sources are identified. Of these sources, 46 were classified as background sources, 11 as H II regions and 6 as supernova remnant candidates. This relatively low number of SNR candidates detected coupled with the low number of large H II regions is consistent with the estimated low star formation rate of the galaxy at $0.06M_{\odot} \text{ year}^{-1}$. Our spectral index map shows that the core of galaxy appears to have a shallow spectral index between $\alpha = -0.2$ and -0.4 . This indicates that the core of the galaxy is a region of high thermal radiation output.

1 Introduction

At ~ 2.08 Mpc (scale of $\sim 10 \text{ pc}''$) away (Dalcanton et al. 2009), NGC 55 is situated between our own Local Group of galaxies and the nearby Sculptor Group

(Karachentsev et al. 2003). The proximity is an advantage as it allows for NGC 55 to be examined in great detail. Previous radio-continuum studies of NGC 55 (Condon et al. 1996; Puche et al. 1991) utilised the Karl G. Jansky Very Large Array (VLA) in compact array configurations as their primary instrument and thus suffer from low resolution. As a result, these studies did not provide source lists of objects within the NGC 55 field.

Until the next generation of radio telescopes such as the Australian Square Kilometre Array Pathfinder (ASKAP), Karoo Array Telescope (KAT & MeerKAT) and the Square Kilometre Array (SKA) become operational, we are restricted to consolidating a selection of NGC 55 radio observations. Part 1 of this paper (Galvin et al. (2012), Paper 1 hereafter) published a new set of highly sensitive and high-resolution radio-continuum images of the NGC 300 field at $\lambda=20$ cm, created by combining data from the Australia Telescope Compact Array (ATCA) and the VLA (also see Payne et al. (2004)). In this paper, we examine all available archived radio-continuum observations of NGC 55 conducted with the ATCA and the VLA at $\lambda=20, 13, 6$ and 3 cm ($\nu=1.4, 2.3, 5.5, 9.0$ GHz) with the intention of merging these observations to create a single radio-continuum image following a similar methodology as presented in Paper 1. By combining a large amount of existing data using the latest generation of computing power we can create new images that feature both high angular resolution and excellent sensitivity. The newly constructed images are analysed and the differences between each map of NGC 55 created at the observed wavelengths are discussed.

In §2 we describe the observational data and reduction techniques. In §3 we present our new maps, a brief discussion and source list is given in §4, and §5 is the conclusion.

Andrew N. O'Brien, Miroslav D. Filipović, Evan J. Crawford, Nicholas F. H. Tothill, Jordan D. Collier, Ain Y. De Horta, Graeme F. Wong, Danica Drašković, Jeff L. Payne

University of Western Sydney, Locked Bag 1797, Penrith, NSW 2751, Australia

Thomas G. Pannuti, Jared P. Napier, Stephen A. Griffith, Wayne D. Staggs

Department of Earth and Space Sciences, Space Science Center, 235 Martindale Drive, Morehead State University, Morehead, KY 40351, USA

Srdjan Kotuš

Department of Physics, University of Novi Sad, Trg Dositeja Obradovića 4, 21000 Novi Sad, Serbia

2 DATA AND DATA REDUCTION

2.1 Observational Data

In order to create a high-resolution and sensitive radio-continuum image, 29 observations from the ATCA and VLA were considered. These observations were selected from the Australian Telescope Online Archive (ATOA) and the National Radio Astronomy Observatory (NRAO) Science Data Archive. The observations which were selected and considered are summarised in Tables 1, 2, 3 and 4.

All ATCA projects, excluding C295, were conducted in mosaic mode with multiple pointings observed. All VLA observations and ATCA project C295 consisted of single pointings of NGC 55. All images are primary beam corrected.

2.2 Data Reduction and Image Creation

To create the best possible NGC 55 mosaic images, we included data from the fixed-position 6th antenna for all ATCA observations, as the large gaps in the uv -plane that dominate compact array configurations were filled mainly with data from observations in other array configurations. The inclusion of these long baselines resulted in images of high resolution with good uv -plane coverage.

The MIRIAD (Sault and Killeen 2006), AIPS (Greisen 2010) and KARMA (Gooch 2006) software packages were used for data reduction and analysis. Because of the large volume of data, the MIRIAD package was compiled to run on a 16-processor high-performance computer system.

MIRIAD was used for all data reduction and imaging, however pre-processing in AIPS was required for the VLA data. This process consisted of importing the data into AIPS using the task FILM, and then splitting the sources into separate datasets with SPLIT. Using the task UVFIX, source coordinates were converted from the B1950 to the J2000 reference frame. The task FITTP was then used to export each source to a FITS file. The MIRIAD task FITS was then used to import these fits files and convert them to MIRIAD files. For the ATCA data, the task ATLOD was used to convert the raw observation files into MIRIAD files.

Typical calibration and flagging procedures were then carried out (Sault and Killeen 2006), including the use of the guided automatic flagging task PGFLAG. Using the task INVERT with a robust weighting scheme, images were created for each ATCA and VLA project separately. Each image was then cleaned using the task

MOSSDI. The MOSSDI task is a SDI clean algorithm designed for mosaic images (Steer et al. 1984). To convolve a clean model the task RESTOR was then used on each of the cleaned maps. These images were created and visually inspected to assess the data quality.

Once the images had been verified to be free of errors, data observed at the same wavelength were combined in the uv -plane as mosaics by using the INVERT and providing the datasets of all observations as the input. This produced 4 dirty maps of all calibrated data of NGC 55 at 20, 13, 6 and 3 cm wavelengths, respectively. These dirty maps were then deconvolved using a more directed approach by providing MOSSDI with boxed regions around each visible source. This method produced superior images which were then restored to produce the combined images. The images were then cropped using IMSUB for analysis so that all images covered the same area of sky ($\sim 0.63^\circ \times 0.41^\circ$) centred at approximately 0h 15m 09s, $-39^\circ 12' 30''$ (J2000).

3 RESULTS

When visually inspecting the images produced from different observations, the effects of the different array configurations is apparent. As mentioned previously, compact arrays produce low resolution images with greater uv -coverage whereas larger arrays produce higher resolution images with less uv -coverage. While point sources are resolved to be much larger at lower resolutions, the advantage of the lower resolution is that they display extended emission throughout the field. This extended emission is lost in the high resolution images. The difference between an image produced using data from a compact array and an image produced using a larger configuration is obvious as can be seen in Figs. 1 and 2. Ideal images are those which have high resolution but also contain extended emission data, which is where the technique of combining observations is advantageous.

After the initial inspection, it was determined that the data from the ATCA project C295 contained very poor uv -coverage and very limited hour angle coverage (0.99 hours). As a consequence, the final image contained several errors. Normally, these errors would disappear or lessen significantly when combined with other data observed in varying array configurations, as the majority of the gaps in the uv -coverage would be filled by the combined data. Since C295 was observed in one of the largest configurations (6C) and was the only observation at this configuration, there was insufficient data to fill the missing uv -coverage. Therefore, the data from C295 was excluded from the final image. Similarly,

Table 1 Summary of VLA and ATCA observations of NGC 55 at $\lambda = 20$ cm used in this study.

Instrument	Project Code	Dates	Array	ν (MHz)	$\Delta\nu$ (MHz)	Primary Calibrator	Secondary Calibrator	Integration Time (h)	Included in Image
VLA	AJ0107:A	23 Mar 1984	BC	1465, 1515	50, 50	0134+329	0008-421	0.68	N
VLA	AC0101:A	13 Jul 1984	CD	1465, 1515	50, 50	0134+329	0025-263	0.12	N
VLA	AS0199:A	29 Aug 1984	D	1465, 1515	50, 50	0134+329	0022-423	0.23	N
VLA	AB0342:A	03 Nov 1985	CD	1465, 1515	50, 50	0134+329	0023-263	0.15	N
VLA	AB0646:A	03 Jul 1992	CD	1465, 1515	50, 50	0134+329	0008-421	2.51	N
VLA	AB0646:B	05 Jul 1992	CD	1465, 1515	50, 50	0134+329	0008-421	2.93	N
ATCA	C1757	18-19 Feb 2009	EW352	1384	128	1934-638	0008-421	61.62	Y
ATCA	C1757	14-21 Nov 2008	EW367	1384	128	1934-638	0008-421	188.00	Y
ATCA	C1757	31 May-01 Jun 2008	EW352	1384	128	1934-638	0008-421	65.57	Y
ATCA	C1612	02-09 Oct 2006	H75	1384	128	0407-658	0008-421	184.10	Y
ATCA	C1341	07-08 Oct 2005	EW214	1384	128	1934-638	0008-421	62.95	Y
ATCA	C1341	18 Jul 2005	H75	1384	128	1934-638	0008-421	21.32	Y
ATCA	C287	25-26 Oct 1995	1.5D	1344	128	1934-638	0008-421	65.07	Y
ATCA	C287	12-13 Jan 1995	375	1380	128	1934-638	0008-421	63.40	Y
ATCA	C287	01-02 Apr 1994	375	1380	128	1934-638	0008-421	54.13	Y
ATCA	C287	01-02 Aug 1993	750D	1380	128	1934-638	0008-421	61.29	Y
ATCA	C295	24 Jun 1994	6C	1380	128	1934-638	0023-263	0.99	N

Table 2 Summary of VLA and ATCA observations of NGC 55 at $\lambda = 13$ cm used in this study.

Instrument	Project Code	Dates	Array	ν (MHz)	$\Delta\nu$ (MHz)	Primary Calibrator	Secondary Calibrator	Integration Time (h)	Included in Image
ATCA	C287	25-26 Oct 1995	1.5D	2378	128	1934-638	0008-421	65.07	Y
ATCA	C287	12-13 Jan 1995	375	2378	128	1934-638	0008-421	63.40	Y
ATCA	C287	01-02 Apr 1994	375	2378	128	1934-638	0008-421	54.13	Y
ATCA	C287	01-02 Aug 1993	750D	2378	128	1934-638	0008-421	61.29	Y

Table 3 Summary of ATCA CABB observations of NGC 55 at $\lambda = 6$ cm used in this study.

Instrument	Project Code	Dates	Array	ν (MHz)	$\Delta\nu$ (MHz)	Primary Calibrator	Secondary Calibrator	Integration Time (h)	Included in Image
ATCA	C2421	15 Mar 2011	1.5A	5500	2048	1934-638	0010-401	27.28	Y
ATCA	C2421	20 Feb 2011	EW352	5500	2048	1934-638	0010-401	26.91	Y
ATCA	C2421	09-10 Nov 2010	750A	5500	2048	1934-638	0010-401	31.04	Y
ATCA	C1974	28 Mar 2010	H168	5600	2048	1934-638	0008-421	136.80	Y
ATCA	C1757	09-10 May 2009	H168	5500	2048	1934-638	0022-423	370.00	Y

Table 4 Summary of ATCA CABB observations of NGC 55 at $\lambda = 3$ cm used in this study.

Instrument	Project Code	Dates	Array	ν (MHz)	$\Delta\nu$ (MHz)	Primary Calibrator	Secondary Calibrator	Integration Time (h)	Included in Image
ATCA	C2421	15 Mar 2011	1.5A	9000	2048	1934-638	0010-401	27.28	Y
ATCA	C2421	20 Feb 2011	EW352	9000	2048	1934-638	0010-401	26.91	Y
ATCA	C2421	09-10 Nov 2010	750A	9000	2048	1934-638	0010-401	31.04	Y

projects C1974 and C1757 were not included in the final 6 cm image because of their low resolution. As all of the 6 cm observations were conducted with the upgraded ATCA Compact Array Broadband Backend (CABB) and, at present, there exists no wide-bandwidth deconvolution algorithm for mosaics in MIRIAD, we had to merge the images in the image plane using IMMERGE. We found that when using this method, the low resolution data appeared to be weighted incorrectly and much of the high resolution data was overwhelmed by the low resolution data. Thus, these data were not used to create the final 6 cm image.

In addition, the VLA observations were also excluded from the final 20 cm image (Fig. 3) as the inclusion of this data overpowered the extended emission from the ATCA observations. Excluding this data was of little consequence as the main advantage of VLA data is the higher resolution, however the largest VLA array configuration used to observe NGC 55 was a single observation in the the BC array which has a maximum baseline separation of approximately 7.6 km. This is relatively close to that of the 6 km maximum baseline at ATCA and so we decided the preservation of the extended emission data was worth more than the slight increase in resolution that would be gained by including the VLA data. Information on the final images used in this paper is given in Table 5.

4 DISCUSSION

4.1 Discrete Sources Within The Field Of NGC 55

A total of 66 sources above 5σ (0.45, 0.92, 0.15, 0.25 mJy/beam at wavelengths of 20, 13, 6 and 3 cm, respectively) were identified within the field of NGC 55. These sources were catalogued by position and flux density. 33 of these sources were detected at more than one of the observed wavelengths and consequently their spectral index, α , was estimated using the equation $S \propto \nu^\alpha$. Simple linear regression was then performed to determine the best-fit value for α between the measured frequencies. This catalogue was then compared to optical (Royal Observatory, Edinburgh et al. 1977), infrared (Dale et al. 2009; Jarrett et al. 2003) and X-ray images (Pannuti et al. 2013; Stobbart et al. 2006) of the NGC 55 field. Source coincidences were accepted for sources within 1 beam of the highest resolution radio image being compared.

Based on their location and comparison with the images at other frequency bands, the sources were classified as either background (BKG) sources, supernova remnants (SNR), or ionised hydrogen regions (H II).

Sources outside of the extended emission boundary seen in Fig. 3 were classified as background sources. Sources inside the boundary were classified as intrinsic (INTR) sources which are further classified as either SNRs or H II regions. If X-ray radiation was detected from the intrinsic source, then it was classified as a SNR candidate since the violent explosions and shockwaves produced by a supernova are known to emit strong X-rays. Also, SNRs usually exhibit steeper spectral index of about $\alpha < -0.5$ (Filipovic et al. 1998). Sources emitting infrared radiation but no detectable X-rays were classified as H II regions. Of the 66 detected radio-continuum sources, 46 were classified as background sources, 11 as H II regions, and 6 as SNR candidates. The full list of sources with positions, flux densities, spectral index and classifications can be found in Table 6.

The low number of detected SNR candidates suggests that the star formation rate for NGC 55 is relatively low. To estimate the high mass star formation rate, we used the relation described by Kennicutt (1983). We adjusted the estimated $H\alpha$ luminosity of NGC 55 given by Hoopes et al. (1996) to 4.08×10^{40} ergs s^{-1} to reflect our adopted distance of 2.08 Mpc. The relation provided estimated high mass star formation rate of $0.06 M_\odot \text{ year}^{-1}$. Compared to the star formation rates of other galaxies in the Sculptor Group (the highest being NGC 253 at $0.20 M_\odot \text{ year}^{-1}$, and the lowest being NGC 45 at $0.01 M_\odot \text{ year}^{-1}$), the star formation rate of NGC 55 is comparatively low.

In Fig. 7 we show the spectral index distribution of all radio-continuum sources found in this study (Table 6; Col. 9). Here, we note that the spectral index alone cannot successfully distinguish between various type of sources. Of the 66 sources reported here, 10 have an estimated spectral index of steeper than -0.85 , classifying them as candidates for compact steep spectrum (CSS) sources (Table 6; Col. 13).

4.2 Spectral Index Map

We show in Fig. 8 an image where each pixel represents the spectral index calculated across all 4 observed frequencies. This image was created based on measurements from Figs. 3, 4, 5 and 6 after convolving the images to the largest beam size. Pixels below the noise level are ignored.

The core of galaxy is shown to have a shallow spectral index of between -0.2 and -0.4 (shown as red pixels). This indicates that the core of the galaxy is a region of high thermal radiation output. The most likely reason for this is that the core of the galaxy is a dense star forming region. The spectral index becomes steeper moving further away from the centre of

Table 5 Image details of ATCA single and merged projects of NGC 55 mosaics at 20, 13, 6 and 3 cm that were used to produce the merged images used for the measurements given in this paper. Merged images were created using joint-deconvolution of all projects.

ATCA Project	Centre ν (MHz)	Synthesised Beam FWHM (")	r.m.s (mJy/beam)	Figure
C287	1362	7.93×4.99	0.09	1
C1341	1384	281.93×188.82	2.13	2
C1612	1384	426.14×279.93	1.08	–
C1757	1384	29.29×24.04	0.99	–
Merged 20 cm	1366	7.94×4.99	0.09	3
C287	2378	18.29×16.96	0.18	4
C2421	5500	5.43×4.68	0.03	5
C2421	9000	5.26×3.62	0.05	6

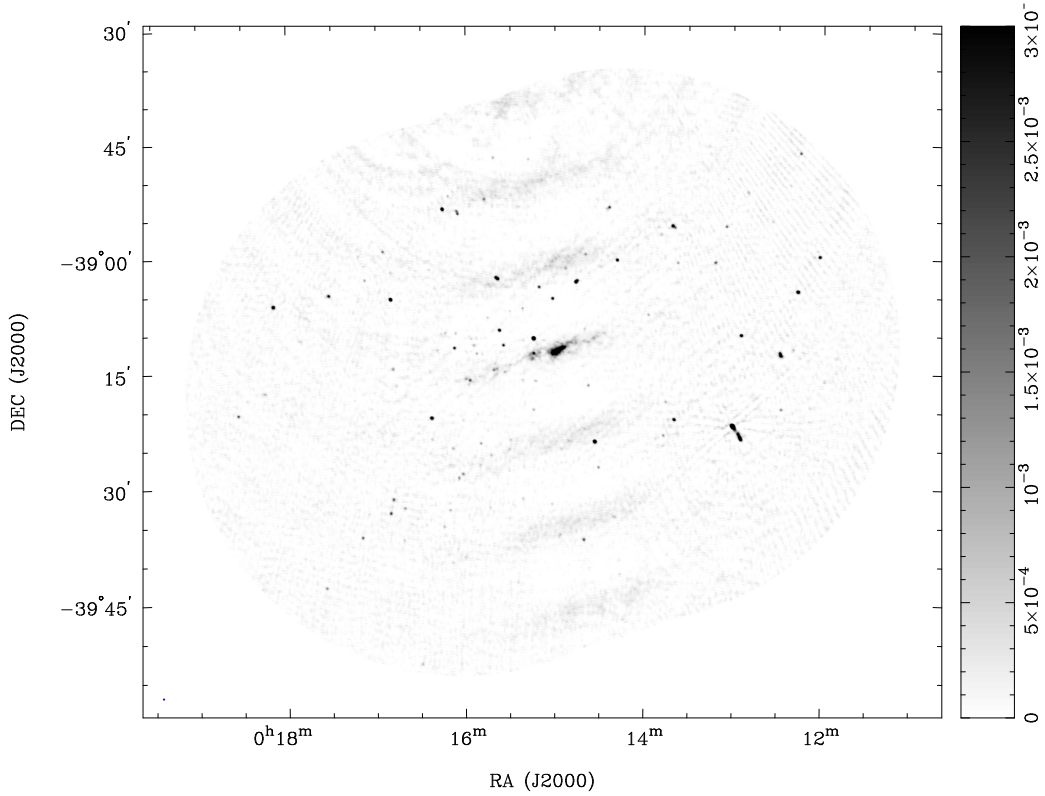


Fig. 1 ATCA Project C287 radio-continuum mosaic of NGC 55 at $\lambda = 20$ cm in Jy/beam. This image illustrates the high resolution produced by observations using a sparse array with long baselines. The synthesised beam is $7.93'' \times 4.99''$ and the r.m.s. noise is 0.09 mJy/beam.

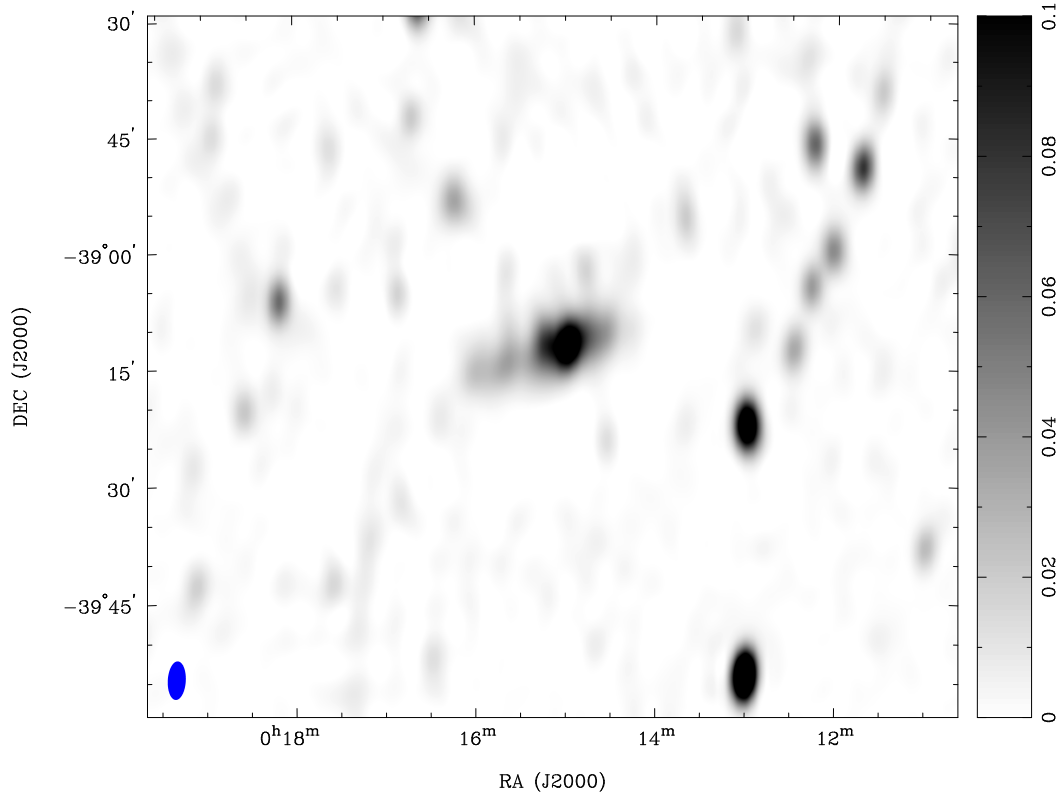


Fig. 2 ATCA Project C1341 radio-continuum mosaic of NGC 55 at $\lambda = 20$ cm in Jy/beam. This image illustrates the low resolution produced by observations using a compact array with short baselines. The synthesised beam is $281.93'' \times 188.82''$ and the r.m.s. noise is 2.13 mJy/beam.

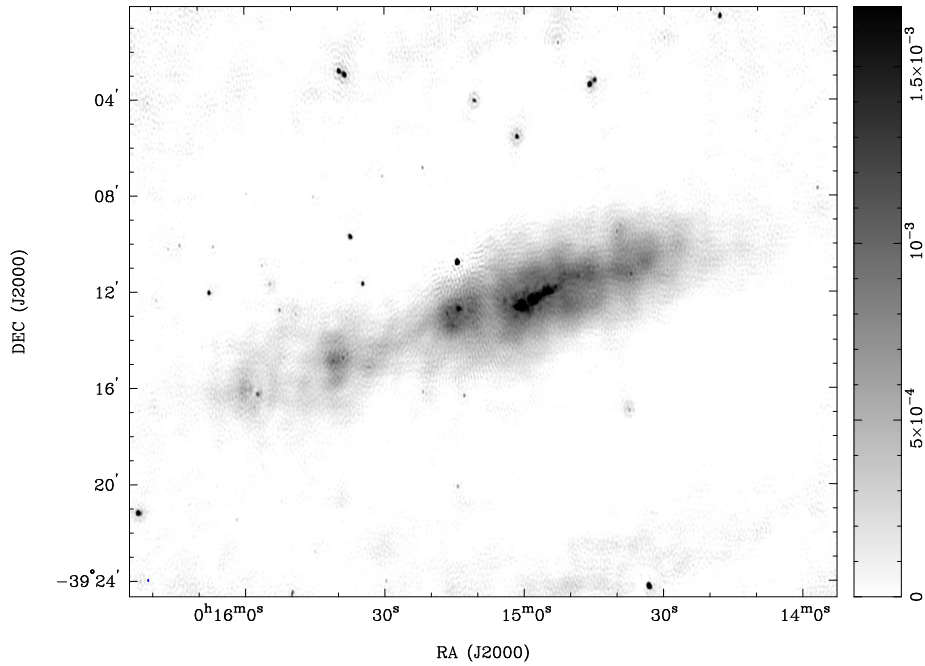


Fig. 3 Cropped total intensity image of all ATCA data (excluding C295) of NGC 55 at $\lambda = 20$ cm in Jy/beam. The synthesised beam is $7.94'' \times 4.99''$ and the r.m.s. noise is 0.12 mJy/beam.

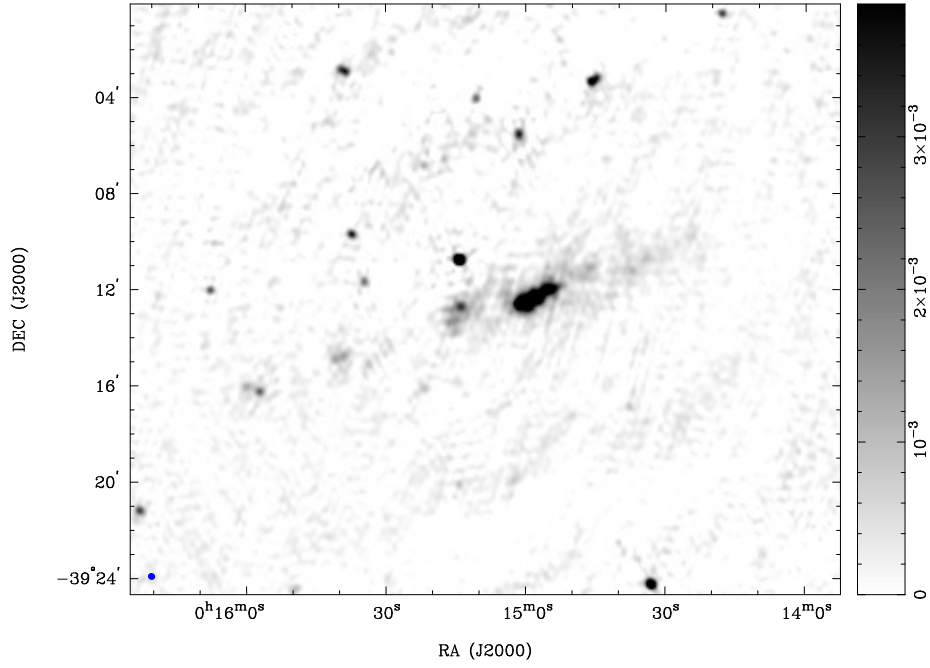


Fig. 4 Cropped total intensity image of all ATCA data of NGC 55 at $\lambda = 13$ cm in Jy/beam. The synthesised beam is $18.29'' \times 16.96''$ and the r.m.s. noise is 0.09 mJy/beam.

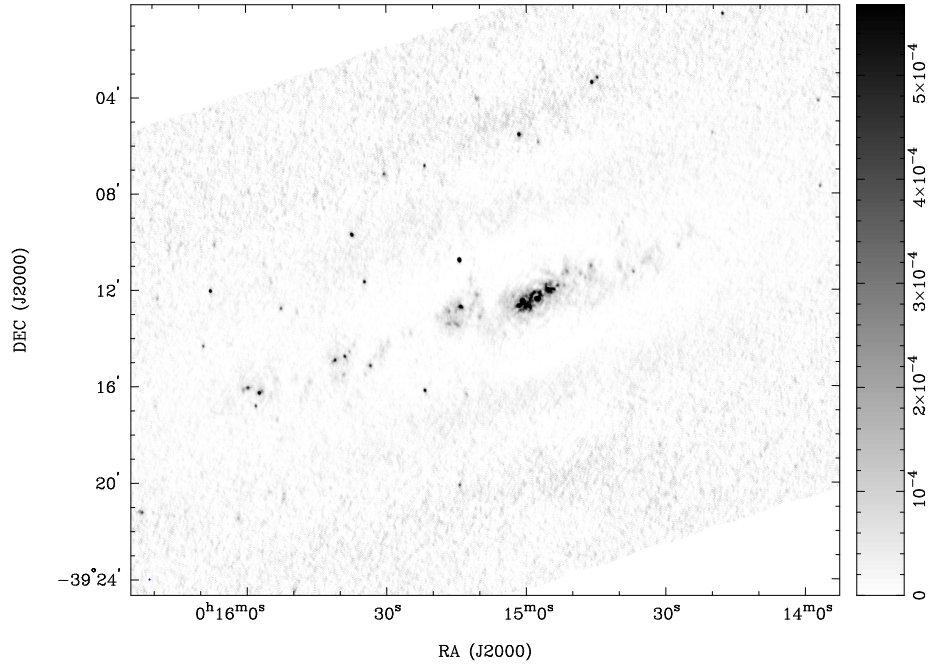


Fig. 5 Cropped total intensity image of all ATCA data of NGC 55 at $\lambda = 6$ cm in Jy/beam. The synthesised beam is $5.43'' \times 4.68''$ and the r.m.s. noise is 0.03 mJy/beam.

Table 6 List of point sources in the NGC 55 field at $\lambda = 20, 13, 6$ and 3 cm. RA (3) and Dec (4) are in J2000 coordinates. Column 9 is the best fit spectral index for all flux measurements of a source. Blank cells indicate no measurement was detected. Asterisks (*) indicate no coverage was available. Daggers (\dagger) indicate sources that were resolved as a single source at $\lambda = 13$ cm but as multiple sources at other wavelengths. These sources were therefore not included in the estimation of α .

1	2	3	4	5	6	7	8	9	10	11	12	13
Index	Source Name	RA (h m s)	Dec ($^{\circ}$ ' '')	S _{20cm} (mJy)	S _{13cm} (mJy)	S _{6cm} (mJy)	S _{3cm} (mJy)	α	Optical ID	IR ID	X-Ray ID	Source Class
1	J001357-390742	00:13:57	-39:07:42	1.05		0.40		-0.69 ± 0.14	*	Y		BKG
2	J001358-390409	00:13:58	-39:04:09			0.41	0.31	-0.55 ± 0.40	*			BKG
3	J001418-390034	00:14:18	-39:00:34	5.47	3.07	0.89		-1.32 ± 0.12	*	Y		BKG (CSS)
4	J001420-390531	00:14:20	-39:05:31			0.21						BKG
5	J001427-391012	00:14:27	-39:10:12			0.15			Y	Y		H II
6	J001430-390129	00:14:30	-39:01:29	0.50					*	Y		BKG
7	J001431-391829	00:14:31	-39:18:29			0.19			Y			BKG
8	J001433-392415	00:14:33	-39:24:15	11.84	10.77			-0.17 ± 0.36	*			BKG
9	J001437-391118	00:14:37	-39:11:18	1.89	1.25	0.37	0.25	-1.13 ± 0.10	Y		Y	SNR
10	J001437-391659	00:14:37	-39:16:59	0.81								BKG
11	J001440-390934	00:14:40	-39:09:34	1.15					Y			H II
12	J001445-390315	00:14:45	-39:03:15	2.96	6.77 \dagger	0.73		-1.01 ± 0.14	*		Y	BKG (CSS)
13	J001446-390327	00:14:46	-39:03:27	6.16	6.77 \dagger	1.82		-0.88 ± 0.14	*			BKG (CSS)
14	J001446-391104	00:14:46	-39:11:04			0.43			Y	Y		H II
15	J001447-391114	00:14:47	-39:11:14		1.96				Y		Y	SNR
16	J001447-391133	00:14:47	-39:11:33			0.20			Y	Y		H II
17	J001448-391123	00:14:48	-39:11:23			0.25			Y			H II
18	J001451-391118	00:14:51	-39:11:18			0.42			Y			H II
19	J001452-391152	00:14:52	-39:11:52			0.32			Y	Y		H II
20	J001453-390142	00:14:53	-39:01:42	0.97					*	Y		BKG
21	J001457-390556	00:14:57	-39:05:56			0.33						BKG
22	J001457-390559	00:14:57	-39:05:59			0.18						BKG
23	J001502-390537	00:15:02	-39:05:37	3.65	4.37	1.88		-0.52 ± 0.36	Y	Y	Y	BKG
24	J001511-390403	00:15:11	-39:04:03	2.19	2.46	0.18		-1.92 ± 0.92	*			BKG (CSS)
25	J001513-391624	00:15:13	-39:16:24	1.10		0.24		-1.09 ± 0.14		Y		BKG (CSS)
26	J001514-391049	00:15:14	-39:10:49	23.31	20.26	13.68	8.80	-0.51 ± 0.08				BKG
27	J001514-391246	00:15:14	-39:12:46	3.51	4.67	1.62	0.89	-0.81 ± 0.27	Y	Y	Y	SNR
28	J001514-392009	00:15:14	-39:20:09	0.88		0.54		-0.35 ± 0.14	*			BKG
29	J001516-391308	00:15:16	-39:13:08	1.38					Y	Y		H II
30	J001518-390736	00:15:18	-39:07:36			0.12			Y			BKG
31	J001522-390655	00:15:22	-39:06:55	0.98	1.25	0.72		-0.26 ± 0.30				BKG
32	J001522-391613	00:15:22	-39:16:13	0.81	1.05	1.14	0.97	0.10 ± 0.10			Y	BKG
33	J001530-390715	00:15:30	-39:07:15	0.58		0.58		-0.01 ± 0.14	Y	Y	Y	BKG
34	J001530-392403	00:15:30	-39:24:03	0.63					*			BKG
35	J001533-391511	00:15:33	-39:15:11	1.00		0.67	0.42	-0.42 ± 0.13	*	Y	Y	SNR
36	J001535-391143	00:15:35	-39:11:43	3.05	2.38	1.02	0.42	-1.04 ± 0.17	*	Y		BKG (CSS)
37	J001537-390946	00:15:37	-39:09:46	4.53	3.88	1.94	0.87	-0.86 ± 0.17	*	Y	Y	BKG (CSS)
38	J001538-390301	00:15:38	-39:03:01	6.32					*			BKG
39	J001538-391437	00:15:38	-39:14:37	1.08		0.22		-1.13 ± 0.14	*			INTR
40	J001539-390258	00:15:39	-39:02:58		4.67				*			BKG
41	J001539-391448	00:15:39	-39:14:48	1.69	2.16 \dagger	0.74	0.43	-0.69 ± 0.10	*	Y		INTR
42	J001539-391533	00:15:39	-39:15:33			0.24			*	Y		H II
43	J001540-390252	00:15:40	-39:02:52	4.97					*	Y		BKG
44	J001540-391452	00:15:40	-39:14:52		2.16				*	Y		H II
45	J001541-391457	00:15:41	-39:14:57	2.03	2.16 \dagger	0.84	0.46	-0.76 ± 0.12	*	Y	Y	SNR
46	J001545-390807	00:15:45	-39:08:07	0.44					*	Y		BKG
47	J001549-391259	00:15:49	-39:12:59	0.59					*	Y		BKG
48	J001550-392429	00:15:50	-39:24:29	1.32	1.21	0.32		-1.07 ± 0.39	*			BKG (CSS)
49	J001552-391248	00:15:52	-39:12:48	1.00		0.51		-0.48 ± 0.14	*	Y	Y	BKG
50	J001552-392029	00:15:52	-39:20:29			0.18			*			BKG
51	J001552-392042	00:15:52	-39:20:42			0.19			*			BKG
52	J001555-391143	00:15:55	-39:11:43	0.67					*			BKG
53	J001556-391057	00:15:56	-39:10:57	0.50					*			BKG
54	J001557-391618	00:15:57	-39:16:18	1.76	2.86	1.43	0.83	-0.46 ± 0.28	*	Y		H II
55	J001558-391650	00:15:58	-39:16:50			0.55	0.33	-1.02 ± 0.40	*	Y		INTR
56	J001600-390758	00:16:00	-39:07:58	0.23					*	Y		BKG
57	J001600-391605	00:16:00	-39:16:05		1.58	0.74	0.27	-1.29 ± 0.30	*	Y	Y	SNR
58	J001602-392128	00:16:02	-39:21:28	0.30		0.22		-0.22 ± 0.14	*	Y	Y	BKG
59	J001607-391009	00:16:07	-39:10:09	0.66		0.28		-0.63 ± 0.14	*		Y	BKG
60	J001608-391203	00:16:08	-39:12:03	3.23	2.63	1.51	0.86	-0.69 ± 0.10	*			BKG
61	J001609-391420	00:16:09	-39:14:20			0.46	0.25	-1.27 ± 0.40	*			BKG (CSS)
62	J001614-391005	00:16:14	-39:10:05	0.73					*			BKG
63	J001616-391014	00:16:16	-39:10:14	0.40					*			BKG
64	J001619-391221	00:16:19	-39:12:21	0.43		0.24		-0.44 ± 0.14	*			BKG
65	J001622-392111	00:16:22	-39:21:11	6.34	3.40	0.63		-1.69 ± 0.24	*			BKG (CSS)
66	J001624-390151	00:16:24	-39:01:51	0.55					*			BKG

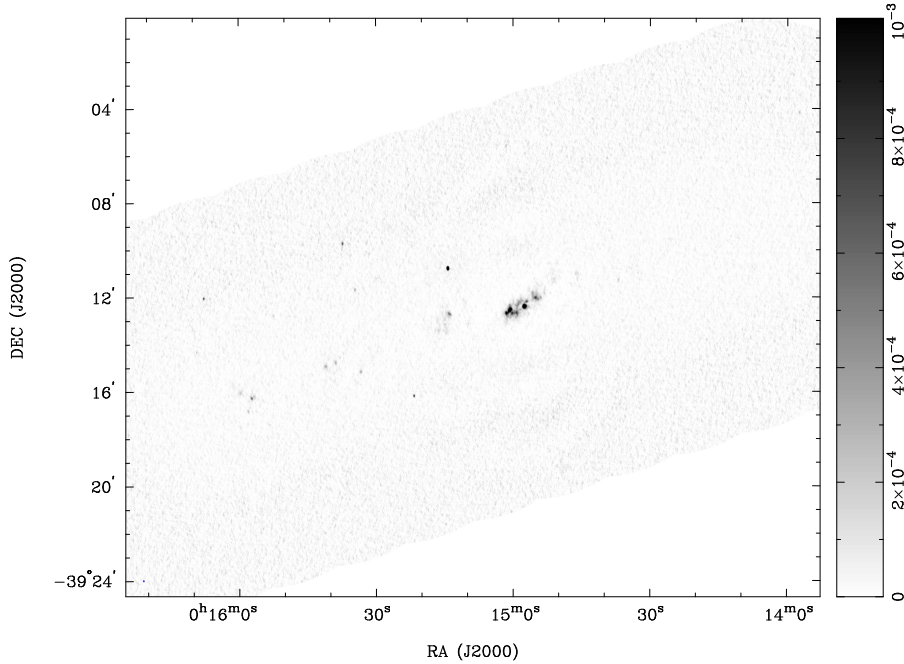


Fig. 6 Cropped total intensity image of all ATCA data of NGC 55 at $\lambda = 3$ cm in Jy/beam. The synthesised beam is $5.26'' \times 3.62''$ and the r.m.s. noise is 0.05 mJy/beam.

NGC 55, indicating a dominance of non-thermal radiation which could be caused by either synchrotron or inverse-Compton radiative mechanisms. Objects which radiate using this mechanism include SNRs and energetic jets.

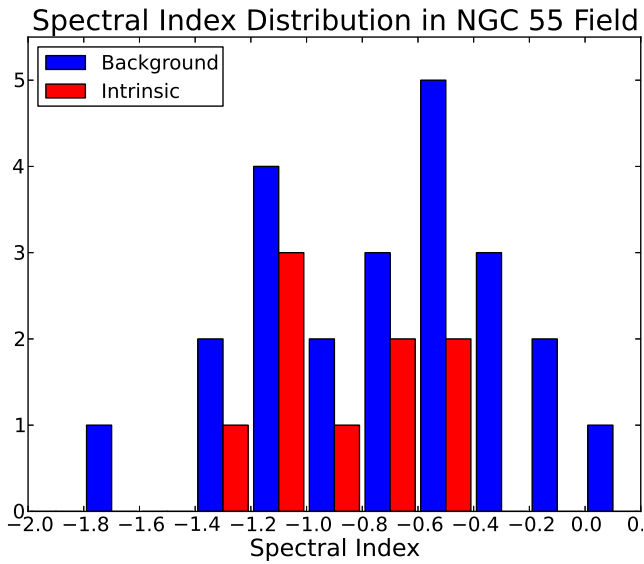


Fig. 7 Histogram of the spectral index distribution of sources in the NGC 55 field with bin widths of 0.2. Sources with high spectral index uncertainties ($> \pm 0.4$) were excluded.

5 CONCLUSION

We present and discuss a series of new highly sensitive, high resolution radio-continuum images of NGC 55 at wavelengths 20, 13, 6 and 3 cm. These images were created by combining data collected from observations using the ATCA radio interferometer telescope. As a result of combining the data, the final images had dramatically reduced levels of noise with higher angular resolution when compared with previous studies. From the new images, a total of 66 radio sources were detected within the field of NGC 55, 33 of which were detected over multiple wavelengths. Of these 66 sources, 46 have been classified as background sources, 11 as H II regions, and 6 as SNR candidates. Spectral indices were also calculated for these multi-wavelength sources. A spectral index map was produced for the galaxy, revealing a high level of thermal radiation emission from the core of the galaxy. Several concentrations of high non-thermal radiation emission were also detected within the plane of the galaxy.

Acknowledgments

The National Radio Astronomy Observatory is a facility of the National Science Foundation operated under cooperative agreement by Associated Universities, Inc. The Australia Telescope Compact Array is part of the Australia Telescope National Fa-

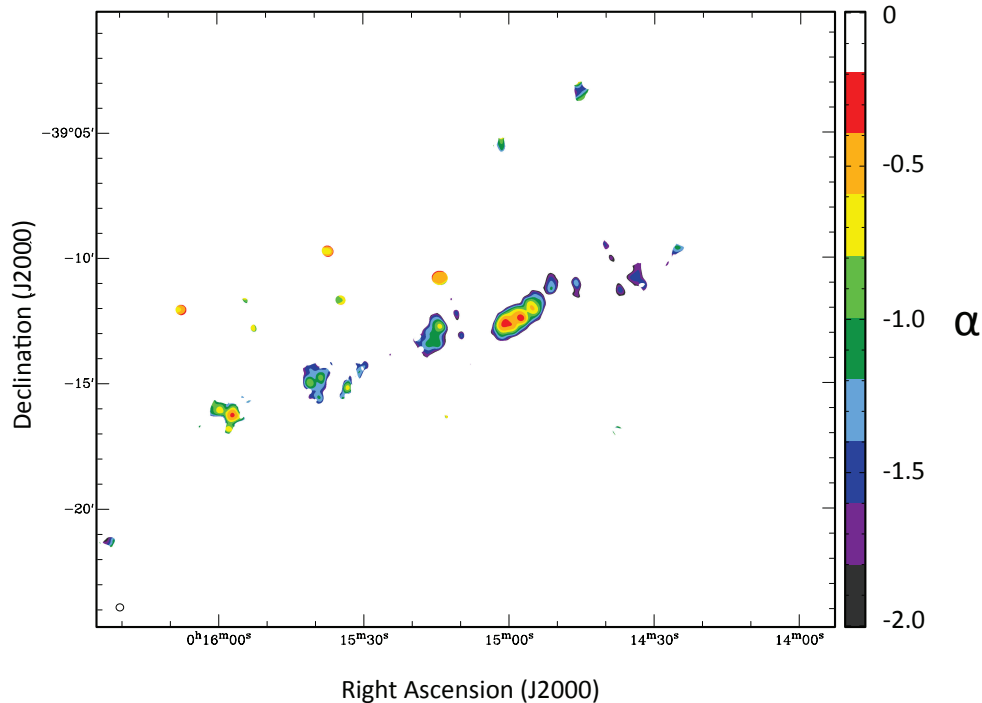


Fig. 8 Spectral index pixel map of NGC 55. Image is in terms of spectral index α . The colour bar on the right reflects the spectral index value multiplied by 1000. The synthesised beam is $18.29'' \times 16.96''$.

cility which is funded by the Commonwealth of Australia for operation as a National Facility managed by CSIRO. This paper includes archived data obtained through the Australia Telescope Online Archive (<http://atoa.atnf.csiro.au>) and the NRAO Science Data Archive (<http://archive.nrao.edu>).

References

- Condon, J.J., Helou, G., Sanders, D.B., Soifer, B.T.: *Astrophys. J. Suppl. Ser.* **103**, 81 (1996)
- Dalcanton, J.J., Williams, B.F., Seth, A.C., Dolphin, A., Holtzman, J., Rosema, K., Skillman, E.D., Cole, A., Girardi, L., Gogarten, S.M., Karachentsev, I.D., Olsen, K., Weisz, D., Christensen, C., Freeman, K., Gilbert, K., Gallart, C., Harris, J., Hodge, P., de Jong, R.S., Karachentseva, V., Mateo, M., Stetson, P.B., Tavares, M., Zaritsky, D., Governato, F., Quinn, T.: *Astrophys. J. Suppl. Ser.* **183**, 67 (2009)
- Dale, D.A., Cohen, S.A., Johnson, L.C., Schuster, M.D., Calzetti, D., Engelbracht, C.W., Gil de Paz, A., Kennicutt, R.C., Lee, J.C., Begum, A., Block, M., Dalcanton, J.J., Funes, J.G., Gordon, K.D., Johnson, B.D., Marble, A.R., Sakai, S., Skillman, E.D., van Zee, L., Walter, F., Weisz, D.R., Williams, B., Wu, S.-Y., Wu, Y.: *Astrophys. J.* **703**, 517 (2009)
- Filipovic, M.D., Haynes, R.F., White, G.L., Jones, P.A.: *Astron. Astrophys. Suppl. Ser.* **130**, 421 (1998)
- Galvin, T.J., Filipović, M.D., Crawford, E.J., Wong, G., Payne, J.L., De Horta, A., White, G.L., Tothill, N., Drašković, D., Pannuti, T.G., Grimes, C.K., Cahall, B.J., Millar, W.C., Laine, S.: *Astrophys. Space Sci.* **340**, 133 (2012)
- Gooch, R.: *Karma Users Guide*. ATNF, Sydney (2006)
- Greisen, E. (ed.): *AIPS Cookbook*. The National Radio Astronomy Observatory, Charlottesville (2010)
- Hoopes, C.G., Walterbos, R.A.M., Greenwalt, B.E.: *Astron. J.* **112**, 1429 (1996). doi:10.1086/118111
- Jarrett, T.H., Chester, T., Cutri, R., Schneider, S.E., Huchra, J.P.: *Astron. J.* **125**, 525 (2003)
- Karachentsev, I.D., Grebel, E.K., Sharina, M.E., Dolphin, A.E., Geisler, D., Guhathakurta, P., Hodge, P.W., Karachentseva, V.E., Sarajedini, A., Seitzer, P.: *Astron. Astrophys.* **404**, 93 (2003)
- Kennicutt, R.C. Jr.: *Astrophys. J.* **272**, 54 (1983)
- Pannuti, T., Napier, J.P., Schlegel, E.M., Laine, S.J., Filipovic, M.D., Griffith, S.A., Staggs, W.D.: In: *American Astronomical Society Meeting Abstracts*. American Astronomical Society Meeting Abstracts, vol. 221, p. 249 (2013)
- Payne, J.L., Filipović, M.D., Pannuti, T.G., Jones, P.A., Duric, N., White, G.L., Carpano, S.: *Astron. Astrophys.* **425**, 443 (2004)
- Puche, D., Carignan, C., Wainscoat, R.J.: *Astron. J.* **101**, 447 (1991)
- Royal Observatory, Edinburgh, European Southern Observatory, Science Research Council (Great Britain): *ESO/SRC Atlas of the Southern Sky*. ESO Sky Atlas Laboratory, Geneva (1977)

- Sault, R., Killeen, N.: *Miriad Users Guide*. ATNF, Sydney (2006)
- Steer, D.G., Dewdney, P.E., Ito, M.R.: *Astron. Astrophys.* **137**, 159 (1984)
- Stobart, A.-M., Roberts, T.P., Warwick, R.S.: *Mon. Not. R. Astron. Soc.* **370**, 25 (2006)